Identification of Squeeze Film Damper Force Coefficients From Multiple-Frequency Noncircular Journal Motions

Adolfo Delgado
e-mail: delgadoa@ge.com

Luis San Andrés
Mast-Childs Professor
Fellow ASME
e-mail: lsanandres@tamu.edu

Department of Mechanical Engineering.
Texas A&M University,
College Station, TX 77843

In rotor-bearing systems, squeeze film dampers (SFDs) provide structural isolation, reduce amplitudes of rotor response to imbalance, and in some instances, increase the system threshold speed of instability. SFDs are typically installed at the bearing supports, either in series or in parallel. In multispool engines, SFDs are located in the interface between rotating shafts. These intershaft dampers must ameliorate complex rotor motions of various whirl frequencies arising from the low speed and the high speed rotors. The paper presents experiments to characterize the forced response of an open ends SFD subject to dynamic loads with multiple frequencies, as in a jet engine intershaft damper. The test rig comprises of a stationary journal and a flexibly supported housing that holds the test damper and instrumentation. The open ends SFD is 127 mm in diameter, 25.4 mm film land length, and has a radial clearance of 0.125 mm. The damper is lubricated with ISO VG 2 oil at room temperature (24 °C, feed pressure 31 kPa). In the experiments, two orthogonally positioned shakers deliver forces to the test damper that produce controlled amplitude motions with two whirl frequencies, one fixed and the other one varying over a specified range that includes the test system natural frequency. The test data collected, forces and motions versus time, are converted into the frequency domain for parameter identification. The identified viscous damping coefficients are strong functions of the amplitude of journal motion, lying within predictions from classical formulas for circular centered orbits and small amplitude motions about an eccentric journal position. The damper inertia coefficients agree well with predictions derived from a fluid flow model that includes the effect of the feed groove. [DOI: 10.1115/1.3159374]

1 Introduction

Squeeze film dampers provide structural isolation, reduce imbalance response amplitude levels in rotating machinery, and in some instances, increase rotor speed stability thresholds. SFDs are common in aircraft gas turbine engines and in some land-based power gas turbines. SFDs are installed at the bearing supports, either in series or in parallel. In the case of multispool engines, SFDs can also be located in the interface between rotating and whirling shafts (see Fig. 1). These dampers, denominated intershaft dampers (ISDs), are subject to whirl motions resulting from the combined imbalance response of both the low speed (LS) rotor and the high speed (HS) rotors. Similarly, in rotating machinery applications incorporating gears, such as in integrally geared compressors, the SFD is subjected to multiple frequency excitations transmitted through the bull gear [1,2]. In both aero gas turbines and compressor applications, the resulting SFD forces and motions are noncircular and with multifrequency components.

Hibner et al. [3–5] conducted early experimental and analytical work on ISDs for multispool gas turbines. Hibner notes that the typical speed ratio (HS/LS) is between 4 and 2 for this type of damper. The author considers the configuration in Fig. 1(*a*), and shows, experimentally and analytically, that this design, in which the squeeze film rotates with the low speed shaft, becomes rotordynamically unstable. Hibner details methods to tune an ISD toward enhancing its stable operation.

El-Shafei [6] also presented a stability analysis of rotors incorporating ISDs and indicated that rotating squeeze films in ISDs, as those shown in Figs. 1(*a*) and 1(*b*), generate a follower force while operating above the system first critical speed that induces unstable operation. The author also introduces a complex though stable intershaft damper design including two ball bearings and two squirrel cages, see Fig. 1(*c*). Unlike the traditional ISD designs, this squeeze film does not rotate but only whirls. Gupta and Chatterjee [7] also test an ISD configuration with two ball bearings (i.e., nonrotating squeeze film) and different combinations of support springs (i.e., attaching the outer race of the damper land to the engine frame) and centralizing springs (i.e., connecting the outer race to the inner race of the damper). The results reveal that the most favorable ISD configuration is the one with centralizing springs. Chen and Liu [8] presented an analysis to predict the response of an ISD for the case where the high and low speed shafts describe synchronous offset elliptical orbits. However, the method is limited to operating conditions with a steady state response for the ideal case (i.e., synchronous vibration of both shafts).

Defaye et al. [9] experimentally evaluated the rotordynamic performance of two ISDs. In the first configuration, as in Fig. 1(*a*), the ISD is installed in the LS shaft, with the film in between the LS shaft and the inner race of a ball bearing that is connected to a squirrel cage, thus, preventing the relative rotation of the squeeze film outer and inner surfaces. The second configuration has the film in between the HS and LS shafts, just as in a hydrodynamic fluid film bearing with the inner and outer cylinders rotating. Rotor motion measurements reveal both ISDs reduce vibration levels but can also lead to unstable rotor operation. In particular, the authors recommend the use of the ISD without a squirrel cage for counterrotating rotors, and further indicate that the ISD with the squirrel cage should be attached to the LS shaft to extend the rotor range of stable operating speeds.

The literature on bearing parameter identification methods is

Manuscript received March 22, 2009; final manuscript received March 29, 2009; published online January 22, 2010. Review conducted by Dilip R. Ballal.

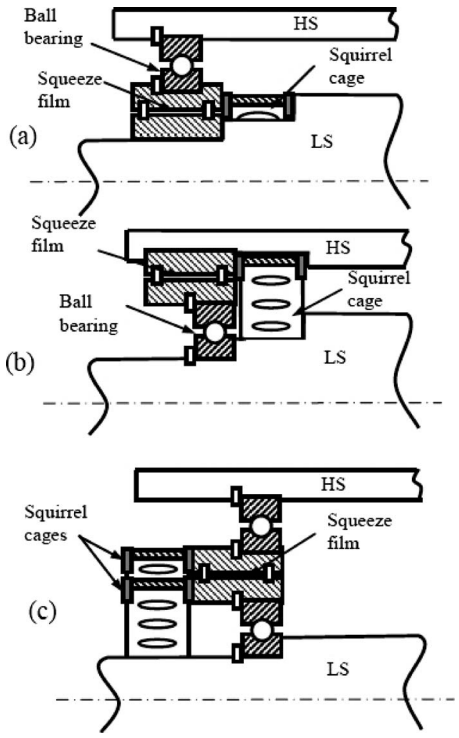

Fig. 1 Schematic view of intershaft damper configurations: (*a*) squeeze film rotates with low speed (LS) rotor, (*b*) squeeze film rotates with pressure high speed (HS) rotor, and (*c*) double ball bearing-squirrel cage design. Reproduced from Ref. [6].

extensive. Tiwari et al. [10] presented a comprehensive review of techniques to characterize the mechanical parameters of fluid film bearings, including different approaches for identifying force coefficients in all type of fluid film bearings, different input excitations, mathematical models, and uncertainty associated to each of the identification methods. Similarly, the identification of force coefficient in SFDs is extensively reported; most works dealing with identification of force coefficients from circular orbits mainly. Della Pietra and Adilleta [11,12] presented most of the relevant analytical and experimental work conducted on SFDs up to 2002. San Andrés and Delgado [13] presented a review of additional experimental work conducted on SFDs from 2002 to date.

In the case of noncircular orbits, El-Shafei and Eranki [14] presented a technique to estimate equivalent force coefficients that best represent the dynamic forced response of a SFD describing elliptic orbits. Equivalent linear force coefficients are obtained from the energy dissipated in terms of the respective system response (i.e., acceleration, velocity, and displacement). The method is applied to estimate the imbalance response of a rotor supported on two squeeze film dampers. El-Shafei uses combinations of force coefficients (mass, stiffness, and damping) to characterize a SFD forced response. One of the models includes a direct (radial) stiffness generated by the squeeze film while ignoring the added mass terms. This approach is not physically consistent since squeeze films do not generate forces proportional to journal static displacements. Zhang and Roberts [15] presented a method to identify force coefficients on a SFD executing both radial and tangential motions about a centered position. The SFD equations of motion and corresponding nonlinear parameters are obtained for radial and circular motions, and a matrix of nonlinear response terms (following a power law form) is constructed. The authors model the damping forces as a polynomial function of the journal displacement including odd and even coefficients. Yet using odd power terms yield a force that both follows and opposes the journal motion in a single period of motion. Thus, such force cannot be dissipative. Furthermore, the authors characterize the response of the damper in terms of ten force coefficients, a rather impractical procedure.

Ellis et al. [16] identified experimentally the force coefficient of a SFD using a time-domain technique. The identification method is based on the state variable filter (SVF) method [17] and relies on solving an auxiliary system of differential equations to obtain the force coefficients of the damper. Although the authors use multifrequency excitations, the SFD coefficients are identified for centered and off-centered journal operation with small dynamic amplitudes to avoid large nonlinear effects.

Diaz and San Andrés [18] presented two methods for the identification of SFD force coefficients from off-centered journal orbits. The first method consists on a least-squares curve fitting of the damping forces in the time domain, and the second one, based on the frequency domain, approximates the measured rotor orbit using its synchronous components (filtered orbit method). The frequency domain method proves to be more adequate and simpler than the time-domain method. The results from the experiments show that the identified damping coefficients are insensitive to whirl frequency and nearly independent of the imbalance magnitude.

San Andrés and De Santiago [19] identified experimentally the damping and added mass coefficients of an open-end squeeze film damper from large amplitude elliptical and circular orbits. The force coefficients are obtained from single frequency excitations following an identification procedure in the frequency domain and neglecting cross-coupled coefficients. The authors investigate the reduction in the film damping capabilities due to air ingestion and entrapment. For the largest test journal orbits, the air entrapment is accounted for as a reduction of the effective length of the damper rather than a reduction in the effective viscosity of the fluid/air film mixture (as represented in previous analytical efforts). The effective length of the SFD is frequency and amplitude dependent, as the amount of air entrapped is a function of these two variables. The identified damping force coefficients for small amplitude orbits agree well with predictions from Ref. [20], except for the identified inertia coefficients that are approximately twice as large as those predicted.

The present work aims to investigate the dynamic response of a SFD subject to multiple frequency whirling motions, similar to those found in the operation of an intershaft SFD. For such motions, the forced response of the damper is nonlinear since the SFD force coefficients are a function of the instantaneous motion amplitude. Presently, damping coefficients are identified from multifrequency sine-sweep excitations over a frequency range that includes the natural frequency of the test system.

2 Test Rig Description

The test rig is the same as that detailed in Ref. [13] for experiments in a SFD with a contacting mechanical end seal. Figure 2 depicts a schematic view of the test rig consisting of a vertical rigid shaft, mounted on three precision ball bearings (natural frequency 400 Hz), and which holds a steel journal 5 in. (127 mm) in diameter and 3 in. (76.2 mm) long. The bearing assembly includes two thick steel plates clamping an acrylic bearing ring. Vertical steel plates, attached to the horizontal plates, serve as interfaces to apply external forces onto the bearing assembly. The top plate includes a lubricant supply connection, a static pressure gauge displaying the feed pressure into the bearing and four eddy current sensors facing the shaft. The composite bearing housing hangs from a top structure with four steel rods providing structural stiffness to the test bearing section. A mechanism atop the test rig, comprising two sliding flat plates (top and bottom support plates), allows adjusting the position of the bearing center with respect to the shaft to simulate centered and off-centered operation conditions.

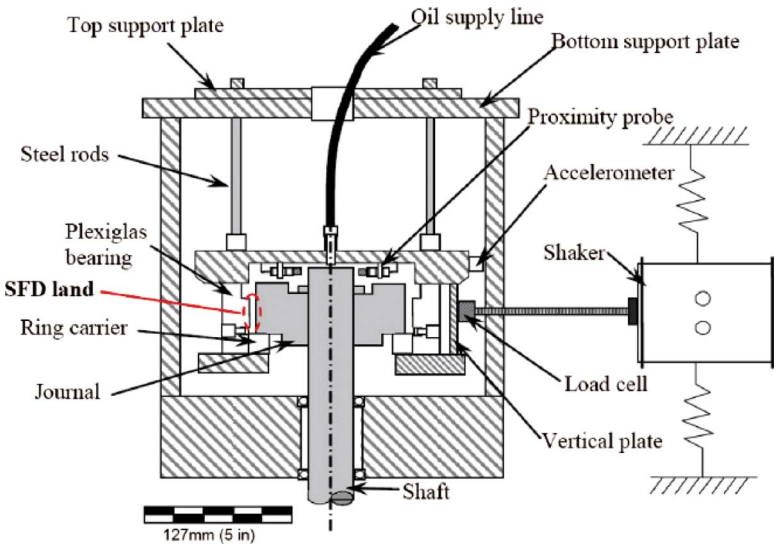

Fig. 2 Schematic view of test rig for SFD dynamic forced response and flow visualization [21]

The bearing housing design integrates a SFD land and inlet groove. Figure 3 depicts a cross section of the test SFD, and details the geometry of the squeeze film land with length $L=25.4$ mm and nominal clearance $c=125$ μm. Presently, the mechanical end seal is not active, and the oil is free to exit the damper through the discharge end groove. Two electromagnetic shakers, suspended from separate steel structures (90 deg apart), excite the test SFD bearing through slender stingers attached to piezoelectric load cells on the bearing housing. A customized data acquisition system records all the sensor signals and controls the electromagnetic shakers.

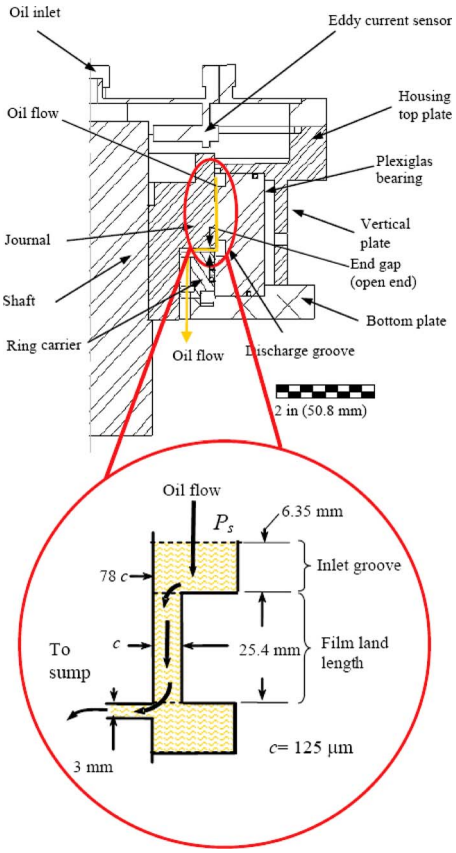

Fig. 3 Cut view of open-end SFD and detail view of squeeze film land

3 Experimental Procedure and Parameter Identification

The shakers excite the test bearing along orthogonal directions with loads of multiple frequency components to reproduce the operation of two shafts whirling with different amplitudes and frequencies, as in a (nonrotating) ISD. Specifically, the SFD is excited with a combination of the load functions

$$F_s(t) = A\ \sin(2\pi f_0 t) + B\ \sin(2\pi f_{1(t)} t)$$
$$F_c(t) = A\ \cos(2\pi f_0 t) + B\ \cos(2\pi f_{1(t)} t) \quad (1)$$

superimposing a single frequency excitation $f_0=25$ Hz representing a LS shaft, and a varying sine-sweep excitation $f_1(t)=(f_I+\Delta f_E t)$ with $f_I=30$ Hz and $\Delta f_E=90$ Hz denoting a HS shaft, for example. Above, A and B are amplitudes of the excitation load. The sine-sweep excitations last 1 s and the sampling frequency is 4096 points/s, i.e., a frequency spectrum with 0.5 Hz step and maximum span of 2 kHz. Table 1 presents the test conditions and lubricant properties.

Figure 4 shows a schematic view of the equivalent mechanical system representation of the SFD. Let $\mathbf{F}_{(t)}=[F_x,F_y]^T$ and $\mathbf{z}_{(t)}=[x,y]^T$ be the vectors of external forces and ensuing bearing displacements, respectively.

The equations of motion for the test bearing section are [13]

Table 1 Test conditions for dynamic load tests with multiple frequencies

Inlet pressure (P_s)	31 kPa (gauge pressure)
Frequency range	25 Hz, 30–120 Hz (sine sweep)
Lubricant temperature (T)	23–25 °C (73–77 °F)
Viscosity (μ) (ISO VG-2)	$3.1-2.8\times10^{-3}$ Pa s
Radial clearance (c)	122–125 μm (4.8–4.9 mil)
Motion amplitude ($\|e\|$)	20–70 μm (0.8–2.9 mil)

$$\mathbf{M_s\ddot{z} + C_s\dot{z} + K_s z = F_{(t)} + F_{SFD(t)}} \tag{2}$$

$$\begin{bmatrix} M & 0 \\ 0 & M \end{bmatrix}\begin{Bmatrix} \ddot{x} \\ \ddot{y} \end{Bmatrix} + \begin{bmatrix} C_{sx} & 0 \\ 0 & C_{sy} \end{bmatrix}\begin{Bmatrix} \dot{x} \\ \dot{y} \end{Bmatrix} + \begin{bmatrix} K_{sx} & 0 \\ 0 & K_{sy} \end{bmatrix}\begin{Bmatrix} x \\ y \end{Bmatrix} = \begin{Bmatrix} F_x \\ F_y \end{Bmatrix} + \begin{Bmatrix} F_x \\ F_y \end{Bmatrix}_{\text{SFD}} \tag{3}$$

where $M=M_s+M_f=10.2$ kg, with M_s as the bearing mass and M_f as the lubricant mass in the plenum atop the squeeze film land. K_{sx} and K_{sy} are the structure support stiffnesses, equal to 860 kN/m and 910 kN/m, respectively, and obtained from impact load tests. $(C_s)_{x,y}$ are the (small) viscous damping coefficients that characterize the energy dissipation from the structural support. From the impact tests, $C_{sx} \sim C_{sy}=130$ N s/m [13].

The SFD forces are of viscous and inertial character, i.e., $\mathbf{F_{SFD}=F_{SFD\text{-}V}+F_{SFD\text{-}I}}$, proportional to the instantaneous speed and acceleration components, i.e.,

$$\mathbf{F_{SFD\_V(}}_{t)} = -\mathbf{C_{SFD}\dot{z}}, \quad \mathbf{F_{SFD\_I(}}_{t)} = -\mathbf{M_{SFD}\ddot{z}} \tag{4}$$

with

$$\mathbf{C_{SFD}} = \begin{bmatrix} C_{\text{SFD}xx(e)} & C_{\text{SFD}xy(e)} \\ C_{\text{SFD}yx(e)} & C_{\text{SFD}yy(e)} \end{bmatrix}, \quad \mathbf{M_{SFD}} = \begin{bmatrix} M_{\text{SFD}xx(e)} & M_{\text{SFD}xy(e)} \\ M_{\text{SFD}yx(e)} & M_{\text{SFD}yy(e)} \end{bmatrix} \tag{5}$$

as the matrices of squeeze film damping and inertia force coefficients, respectively. Above, $e_{(t)}$ is the journal instantaneous eccentricity $\sqrt{(x^2+y^2)}$. For the range of test eccentricities or orbit amplitudes, up to $\sim$60% (70 μm) of the damper clearance c, the added mass coefficients are mainly due to temporal fluid inertia effects and, thus, can be approximated to constant magnitudes [22]. On the other hand, the squeeze film viscous damping coefficients are strong nonlinear functions of the journal eccentricity, as noted in Eq. (5) [23].

The input load excitations and ensuing bearing displacements are expressed as

$$\mathbf{F}_{(t)} = \sum_{k=1}^{m} \begin{Bmatrix} \bar{F}_{x_k} \\ \bar{F}_{y_k} \end{Bmatrix} e^{i\omega_k t} = \sum_{k=1}^{m} \bar{\mathbf{F}}_k e^{i\omega_k t}$$

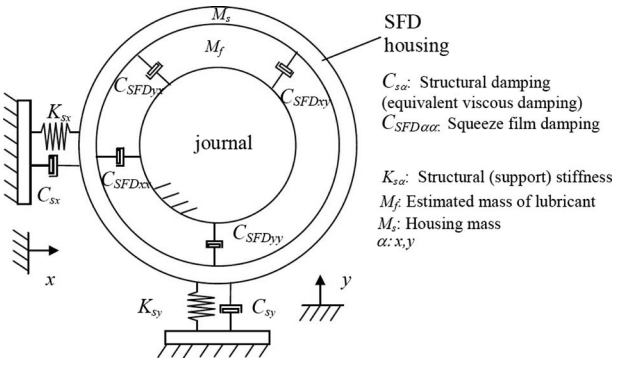

Fig. 4 Equivalent representation of test SFD with mechanical parameters

$$\mathbf{z}_{(t)} = \sum_{k=1}^{m}\sum_{j=1}^{n} \begin{Bmatrix} \bar{x}_{(2j-1)_k} \\ \bar{y}_{(2j-1)_k} \end{Bmatrix} e^{i\omega_k jt} = \sum_{k=1}^{m}\sum_{j=1}^{n} (\bar{\mathbf{z}}_{(2j-1)_k} e^{i\omega_k jt}) \tag{6}$$

where $(\bar{F}_{x_k}, \bar{F}_{y_k})$ and $(\bar{x}_{j_k}, \bar{y}_{j_k})$ are the components of the discrete Fourier transform (DFT) of the time varying force and displacement vectors, respectively. Note that the DFT of the force input does not include multiple harmonics of the excitation frequency (ω_k). On the other hand, due to the nonlinear nature of the squeeze film damping force, the frequency spectrum of a displacement contains multiple harmonics $(\omega_k, 3\omega_k, 5\omega_k, \ldots)$.[1] For the excitation in Eq. (1), undiscerning harmonic components $(\omega_k=3\omega_j)$ occur for frequencies above $\sim$75 Hz (i.e., 3$\times$ lowest frequency). Thus, for all test conditions, useful identification of parameters is limited to the range 40–75 Hz.

The squeeze film damping force is nonlinear and expressed in the frequency domain as the superposition of multiple frequency components

$$\begin{aligned} \mathbf{F_{SFD\_V}}(e,\omega,\dot{\mathbf{z}}) = {} & \boldsymbol{\gamma}_{1_k}(\bar{\mathbf{z}}_{1_k}\omega_k)e^{\omega_k t} + \boldsymbol{\gamma}_{2_k}(\bar{\mathbf{z}}_{3_k}3\omega_k)e^{3\omega_k t} + .. \\ & + \boldsymbol{\gamma}_{n_k}(\bar{\mathbf{z}}_{(2n-1)_k}(2n-1)\omega_k)e^{(2n-1)\omega_k t} \end{aligned} \tag{7}$$

where the terms in parenthesis are proportional to each of the velocities in the frequency domain. Note, however, that the only frequency component of the squeeze film force that dissipates mechanical energy is the synchronous one (ω_k), since the work input into the system is related to the fundamental frequency [21]. Thus, the squeeze film damping coefficient corresponds to the first frequency component of the dissipative force, i.e., $C_{SFD\alpha\beta} = \gamma_{1\alpha\beta_k}, \quad \alpha,\beta: x,y$.

Substituting Eq. (6) into Eq. (3) for each of the fundamental frequency components (ω_k) of the sine-sweep excitation force yields

$$\begin{aligned} \bar{F}_{x_k} &= (H_{xx}\bar{x} + H_{xy}\bar{y})_k \\ \bar{F}_{y_k} &= (H_{yy}\bar{y} + H_{yx}\bar{x})_k \end{aligned} \tag{8}$$

where the impedance functions are

$$H_{\alpha\beta_k} = K_{s\alpha\beta} - M_{s-\alpha\beta}\omega_k^2 + i\omega_k C_{s-\alpha\beta}, \quad \alpha,\beta = x,y \tag{9}$$

with test *system* mass and damping coefficients defined as

$$\begin{aligned} M_{s-\alpha\alpha} &= M_{\text{SFD}\alpha\alpha} + M \\ C_{s-\alpha\alpha_k} &= C_{\text{SFD}\alpha\alpha_k} + C_{s\alpha}, \quad C_{s-\alpha\beta_k} = C_{\text{SFD}\alpha\beta_k}, \quad \alpha,\beta = x,y \end{aligned} \tag{10}$$

As previously noted, the system damping coefficients $(C_{s-\alpha\beta})$ are a function of the frequency, since the displacement amplitude also varies with frequency. Thus, the damping coefficients in Eq.

[1] As verified with single frequency load excitations. For a single frequency excitation force, the ensuing damper displacement presents multiple harmonic components (1$\times$ and 3$\times$ predominantly).

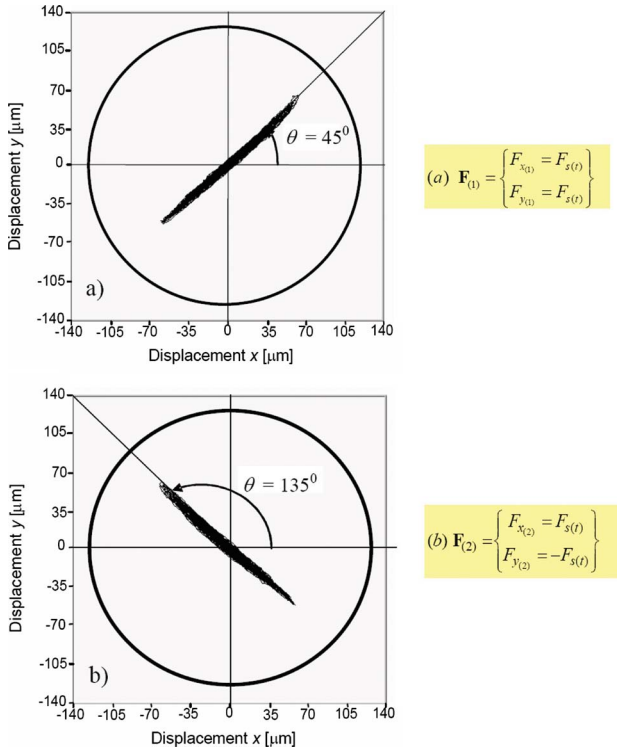

$$(a)\ \mathbf{F}_{(1)} = \begin{Bmatrix} F_{x_{(1)}} = F_{s(t)} \\ F_{y_{(1)}} = F_{s(t)} \end{Bmatrix}$$

$$(b)\ \mathbf{F}_{(2)} = \begin{Bmatrix} F_{x_{(2)}} = F_{s(t)} \\ F_{y_{(2)}} = -F_{s(t)} \end{Bmatrix}$$

Fig. 5 Measured bearing orbits (*y* versus *x*) due to two fixed amplitude load vectors (*a*) $\mathbf{F}_{(1)}$ and (*b*) $\mathbf{F}_{(2)}$. Multifrequency excitation (constant 25 Hz+sine-weep 30–120 Hz). Damper clearance circle noted.

(9) cannot be estimated with a single parameter, as in the case of circular journal motions about a centered position, see, for example, Ref. [13].

In the experimental procedure, the impedance functions ($H_{\alpha\beta}$) are determined from two linearly independent excitation vectors using a combination of the multiple frequency sine-sweep excitation loads in Eq. (1).

4 Results: Dynamic Response and Identified Force Coefficients

4.1 Multiple Sine-Sweep Excitation With Fixed Force Amplitudes. To identify the SFD four damping coefficients and four added mass coefficients, two force vectors generating linearly independent motions are required. A pair of excitation force vectors that meet these conditions is

$$\mathbf{F}_{(1)} = \begin{Bmatrix} F_{x_{(1)}} = F_{s(t)} \\ F_{y_{(1)}} = F_{s(t)} \end{Bmatrix}, \quad \mathbf{F}_{(2)} = \begin{Bmatrix} F_{x_{(2)}} = F_{s(t)} \\ F_{y_{(2)}} = -F_{s(t)} \end{Bmatrix} \tag{11}$$

with $F_{s(t)}$ as in Eq. (1), $A=15$ N and $B=150$ N are held constant. Figure 5 depicts graphs with the journal displacement paths (y versus x) induced by each excitation vector. $\mathbf{F}_{(1)}$ renders multifrequency motions enclosed within elliptical envelope trajectories with the mayor axis oriented along $\theta=45$ deg. Similarly, $\mathbf{F}_{(2)}$ induces elliptical motions at $\theta=135$ deg from the X direction.[2] Figure 6 shows a representative time trace of the excitation forces and ensuing motions in both directions when exciting the system with $\mathbf{F}_{(1)}$. Figure 7 depicts the DFT of the loads and ensuing displacements presented in Fig. 6. The frequency spectra show a fixed excitation frequency (25 Hz) and the sine-sweep excitation (30–120 Hz).

[2]In an intershaft system, this condition simulates the case where the motion response vector for each shaft is in phase and out of phase with each other.

Table 2 SFD inertia force coefficients identified from fixed amplitude, (40–75 Hz) sine-sweep loads

Parameter	*xx*	*Yy*
Identified mass (M_{s-})	16.3 kg	16.1 kg
Squeeze film inertia (M_{SFD})	6.1 kg	5.9 kg
r^2 (goodness of curve fit)	0.97	0.98
System mass (M_s) (kg)[a]	9.6	
Fluid mass (M_f) (kg)[a]	0.62	
Added mass coefficient (predictions from Ref. [24])	6.6 kg	

[a]Measured independently [13].

The identified impedance functions follow from

$$\begin{bmatrix} H_{xx} & H_{xy} \\ H_{yx} & H_{yy} \end{bmatrix} = \left[\bar{\mathbf{F}}_{(1)} \quad \bar{\mathbf{F}}_{(2)}\right]\left[\bar{\mathbf{z}}_{(1)} \quad \bar{\mathbf{z}}_{(2)}\right]^{-1} \tag{12}$$

where $\bar{\mathbf{z}}_{(i)}$ represents the displacement vector due to the corresponding excitation load vector. The system impedance functions are identified and averaged from 30 sets of excitations $\mathbf{F}_{(1)}$ and $\mathbf{F}_{(2)}$. This procedure is repeated three times to yield a single average set of impedance functions.

The stiffness and added mass coefficients are identified from the real part of the impedance functions, Eq. (9), using a quadratic curve fit in terms of the frequency

$$K_{s\alpha\beta} - \omega_k^2 M_{\mathrm{SFD}\alpha\beta} = \mathrm{Re}(H_{\alpha\beta_k}), \quad \alpha,\beta = x,y \tag{13}$$

The damping coefficients follow from the imaginary part of the impedance function divided by the excitation frequency,

$$C_{\mathrm{SFD}\alpha\beta_k} = \frac{\mathrm{Im}(H_{\alpha\beta_k})}{\omega_k} - C_{s\alpha\beta}, \quad \alpha,\beta = x,y \tag{14}$$

Figure 8 depicts the real and imaginary parts of the identified direct impedance function (H_{xx}). Figure 8(*a*) shows the corresponding curve fit of the dynamic stiffness ($K_{s\alpha}-M_{s-\alpha\alpha}\omega^2$, $\alpha=x,y$), and Fig. 8(*b*) shows the damping coefficient ($C_{\mathrm{SFD}xx}$), as defined in Eq. (14). Table 2 presents the identified system and squeeze film added mass coefficients. The table also shows the predicted coefficient using the model in Ref. [24], which takes into account the effect of the inlet groove on the dynamic forced response of the damper. The cross-coupled force coefficients, not shown for brevity, are rather small (less than 5% of the identified direct coefficients) as expected for SFD operation in the absence of oil cavitation. Figure 8(*b*) shows that the damping coefficient ($C_{\mathrm{SFD}xx}$) decays throughout the frequency identification range with a similar trend to that shown in the frequency spectrum of the journal displacement in Fig. 7(*b*). This is, as expected, a clear indication of the dependency of the damping coefficient on the amplitude of motion.

Figure 9 presents the identified direct damping coefficients $C_{\mathrm{SFD}xx}$ and $C_{\mathrm{SFD}yy}$. The figure also includes predictions from classical theory [20] for two cases: circular centered orbits (CCOs) and radial motions about an off-centered journal position (ORMs - off-centered radial motions). Since the multiple frequency excitations exert a combination of radial and circumferential journal motion paths, the damping coefficients are expected to lie within the region enclosed between the limiting cases.

4.2 Sine-Sweep Excitations With Varying Force Amplitude. Cross-coupled force coefficients are negligible for the test SFD since it operates without lubricant cavitation. Presently, the principal force coefficients (xx and yy) can be obtained directly from journal displacements induced by the force vector

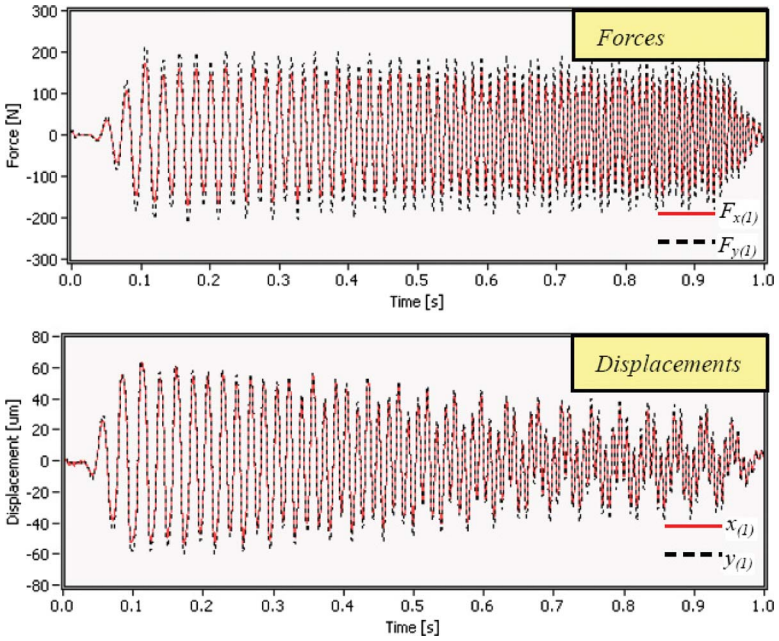

Fig. 6 Time traces of excitation force vector $\mathbf{F}_{(1)}$ and ensuing $x_{(t)}$ and $y_{(t)}$ bearing displacements. Fixed amplitude load. Multifrequency excitation (constant 25 Hz+sine sweep 30–120 Hz). Maximum motion amplitude ~60 μm. Damper radial clearance c=0.125 mm.

$$\mathbf{F}_{(3)} = \begin{Bmatrix} F_{x_{(3)}} = F_{c(t)} \\ F_{y_{(3)}} = F_{c(t)} \end{Bmatrix} \tag{15}$$

with $F_{s(t)}$ and $F_{c(t)}$ defined in Eq. (1). Three independent tests are conducted with load amplitudes B that increase linearly with time. Specifically, the load coefficients A and B in Eq. (1) are

$$A = \begin{pmatrix} 2.5 \\ 5 \\ 15 \end{pmatrix} N, \quad B = \begin{pmatrix} 5 + 50t \\ 10 + 100t \\ 25 + 250t \end{pmatrix} N \tag{16}$$

The aim is to induce journal motions, x and y, of nearly constant or fixed amplitude irrespective of the excitation frequency. Figure 10 depicts the time transient variation in the applied force vector $\mathbf{F_3}$ and the ensuing bearing motions with amplitude of ~50 μm

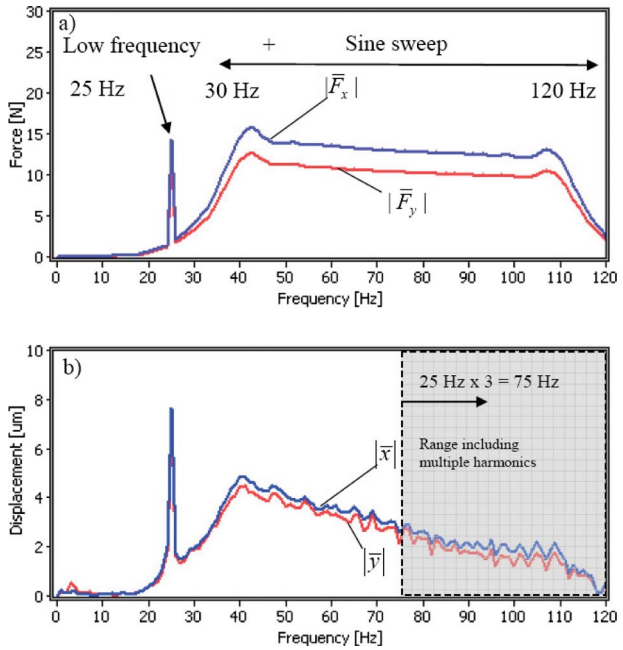

Fig. 7 DFTs of input force vector $\mathbf{F}_{(1)}$ and ensuing x and y displacements

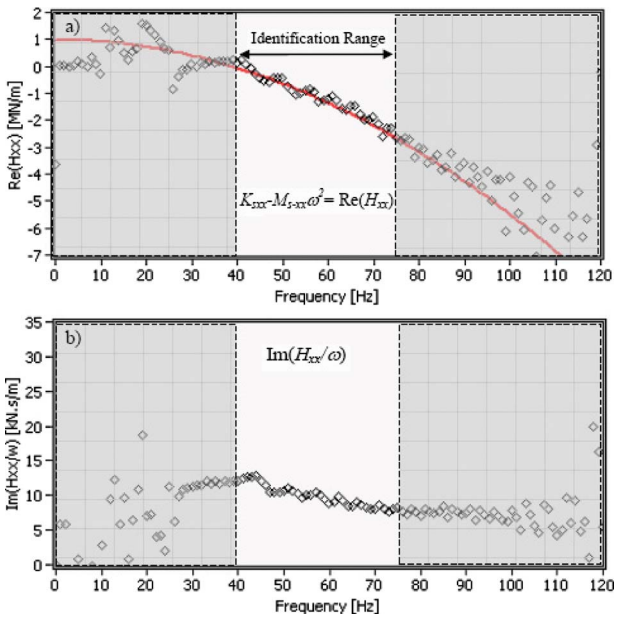

Fig. 8 Real and imaginary parts of direct impedance function H_{xx} versus frequency. Fixed load amplitude. Multiple frequency excitation (constant 25 Hz+sine sweep 30–120 Hz).

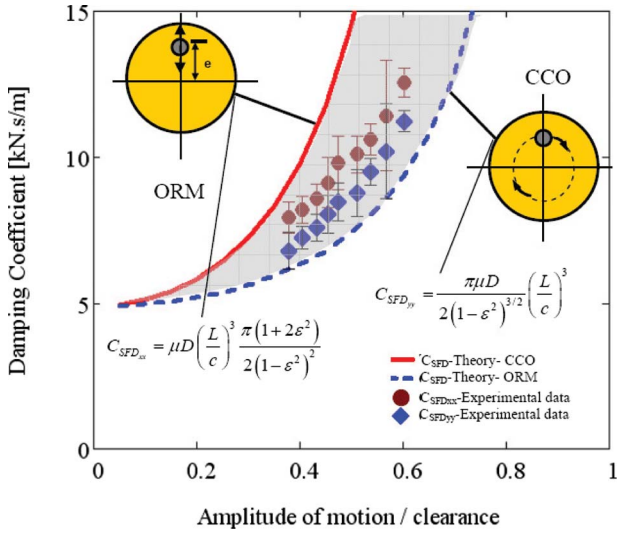

Fig. 9 Squeeze film damping coefficients identified from fixed load amplitude—multifrequency sine-sweep forced excitations (constant 25 Hz+sine sweep 30–120 Hz). Predictions for circular centered orbits (CCO) and radial motions about an off-centered journal static position (ORM).

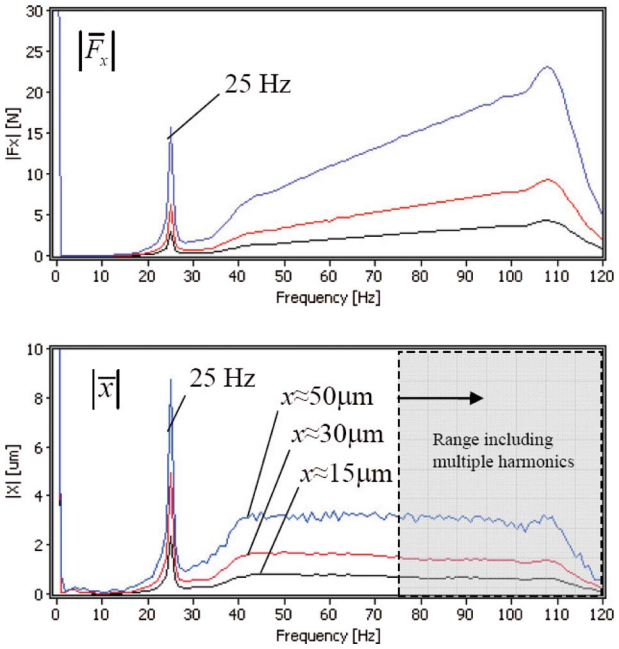

Fig. 11 DFTs of input force and ensuing *x*-displacement. Time data shown in Fig. 10. Three load conditions giving approximately constant motion amplitudes. Excitation force vector $\mathbf{F}_{(3)}$.

along the X and Y directions. Figure 11 depicts the DFTs of the applied x-direction forces generating constant amplitude displacements of ~15 μm, 30 μm, and 50 μm. The bottom graph shows that for frequencies above 75 Hz, nondiscernible multiple frequency responses occur.

Figure 12 depicts the imaginary part of the direct impedance function (H_{xx}) obtained from tests with sine-sweep excitation loads of increasing force amplitude. The results show that the imaginary part of H_{xx} can be approximated with a linear fit in frequency. Thus, direct damping coefficients of constant magnitude are readily identified from the slope of the curve fit, i.e.,

$$\mathrm{Im}(H_{\alpha\beta}) - \omega C_{s\alpha\beta} = \omega(C_{\mathrm{SFD}\alpha\beta}), \quad \alpha,\beta = x,y \tag{17}$$

The test results reveal that the damping can be represented with a single parameter as long as the amplitude of journal motion is constant throughout the identification frequency range. Table 3 presents the system identified mass coefficients (M_{s-xx}, M_{s-yy}) and squeeze film added mass coefficients ($M_{\mathrm{SFD}xx}, M_{\mathrm{SFD}yy}$). The iden-

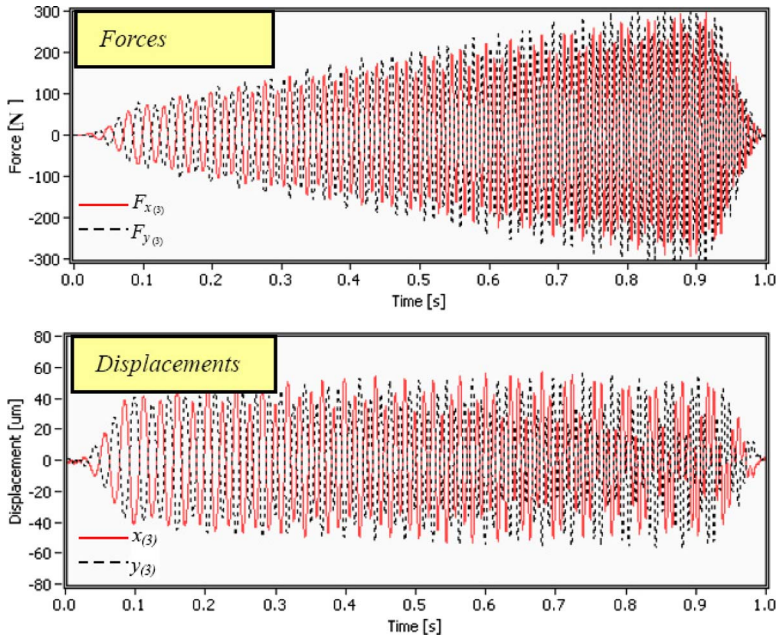

Fig. 10 Time traces of excitation force vector $\mathbf{F}_{(3)}$—varying amplitude—and ensuing $x_{(t)}$ and $y_{(t)}$ bearing displacements. Multifrequency excitation (constant 25 Hz+sine sweep 30–120 Hz). Maximum motion amplitude ~50 μm, damper radial clearance c=0.125 mm.

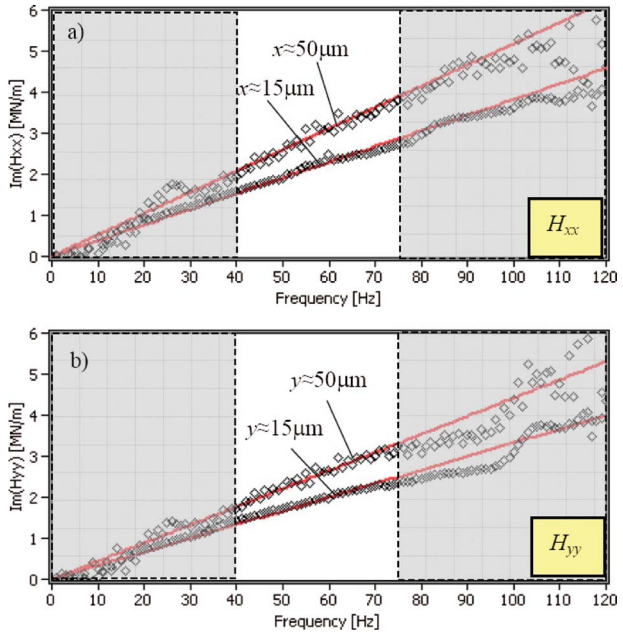

Fig. 12 Imaginary part of impedances H_{xx} and H_{yy} derived from two load conditions giving approximately constant displacement amplitudes: 15 μm and 50 μm

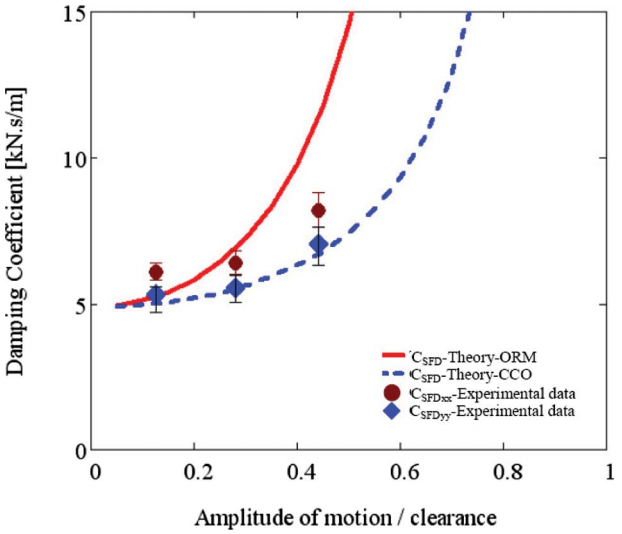

Fig. 13 Squeeze film damping coefficients identified from varying load amplitude—multifrequency sine-sweep forced excitations (constant 25 Hz+sine sweep 30–120 Hz). Predictions for circular centered orbits (CCO) and radial motions about an off-centered journal static position (ORM).

tified added mass coefficients are similar to those in Table 2, and also correlate well with the predicted value of 6.6 kg given in Ref. [24].

Table 4 presents the damping coefficients identified from the sine-sweep load excitations ensuing nearly constant amplitude bearing motions. The uncertainty associated to the estimated squeeze film damping coefficient (i.e., slope of curve fit) is presented for a 95% confidence interval, as in Ref. [25].

Figure 13 depicts the damping coefficients identified from the excitation force with varying amplitude. The figure also includes the predicted damping coefficients for circular centered orbits and radial motions about an off-centered journal position. The identified damping coefficients for the largest test journal amplitude are slightly smaller (~20%) than those detailed in the previous section for a fixed load amplitude. A small discrepancy is expected since for both experiments the bearing follows different motion paths. Furthermore, the motions exerted by the fixed load excitation include larger variations of the journal motion amplitude (i.e., motions along the radial direction) when compared with the tests with increasing load amplitudes and relatively constant journal motions amplitude. In addition, the constant load amplitude excitation tests also yield larger amplitude motions at lower frequencies than when exciting the system with varying (increasing) load excitations. Although the maximum peak force in both experiments is similar at the highest frequencies, at low frequencies the constant excitation test yield larger amplitude motions not induced during the variable amplitude load tests.

Table 3 SFD inertia coefficients identified from varying load amplitude, (40–75 Hz) sine-sweep forces

Max. displacement amplitudes $\|x\|$, $\|y\|$	20 μm	40 μm	60 μm	r^2
M_{s-xx}	16.1kg	16.1kg	16.2kg	0.99
M_{SFDxx}		5.9 kg		
M_{s-yy}	15.8kg	15.9kg	16.1kg	0.99
M_{SFDyy}		5.8 kg		

r^2(goodness of curve fit).

Table 4 Damping coefficients estimated from constant displacement amplitude tests induced by varying amplitude sine-sweep excitation loads

Amplitude (μm)	15	30	50
C_{SFDxx} (N s/m)	6100(±300)	6400(±400)	8200(±600)
C_{SFDyy} (N s/m)	5300(±600)	5500(±500)	7000(±700)

Uncertainties noted.

5 Conclusions

SFD force coefficient (damping and inertia) are identified from noncircular multiple frequency motions. The multiple frequency excitations and operating conditions intend to replicate those of dampers in integrally geared compressors and of double squirrel cage SFD in an air-breathing gas turbine engine, for example. Note, however, the experimental SFD hardware does not replicate a typical intershaft damper.

The experiments show that the SFD damping coefficients can be obtained from system impedance functions that consider only the frequency component that coincides with the forced excitation frequency, since this is the only component that dissipates mechanical energy. The identified cross-coupled coefficients are negligible, which confirms that the damper operates without oil cavitation.

The forcing functions include a constant frequency excitation (25 Hz), simulating a low speed shaft, and a sine-sweep excitation, from 30 Hz to 120 Hz, representing the excitation in a high speed shaft. The tests include forced excitation with a fixed load amplitude and a varying load amplitude in time. For the case of constant amplitude of the excitation force, the ensuing displacement amplitude decays steadily with frequency, and the identified viscous damping coefficients are strong functions of the amplitude of journal motion and frequency. For the case that the excitation force amplitude increases as the excitation frequency increases, the resulting displacement amplitude is relatively constant through the identification frequency range. For such excitation conditions, regardless of the journal motion path, the damping coefficients can be obtained with a single frequency independent coefficient. The identified added mass coefficients are large though agreeing

well, ~15% difference, with predictions from an improved fluid inertia model that accounts for the inlet groove [24]. The experimental squeeze film damping coefficients are bracketed by predicted values from circular centered orbits and small amplitude motions about an eccentric journal position.

Acknowledgment

The continued support from the TAMU Turbomachinery Research Consortium is gratefully acknowledged. The authors also thank Honeywell Engines, Systems, and Services (Phoenix) for their support and interest on this research work.

Nomenclature

A, B = amplitudes of load excitation (N)
F_s, F_c = excitation periodic loads, multiple frequency (N)
$f_0,$ = low frequency excitation (Hz)
$f_I, f_E,$ = start and end frequencies of sine-sweep function, $\Delta f_E = f_E - f_I$ (Hz)
c = squeeze film radial clearance (m)
$C_{sx} = C_{sy}$ = support structure damping coefficients (N s/m)
$C_{\mathrm{SFD}\alpha\beta}$ = squeeze film damping coefficients (N s/m) $\alpha, \beta = x, y$
D = $2R$, journal diameter (m)
e = $\sqrt{(x^2+y^2)}$, journal eccentricity (m)
F_x, F_y = external forces applied to test bearing system (N)
$\bar{F}_x, \bar{F}_y$ = DFT components of applied forces (N)
$H_{\alpha\beta}$ = test system impedance functions (N/m), $\alpha, \beta = x, y$
K_{sxx}, K_{syy} = support structure stiffnesses (N/m)
L = length of squeeze film land (m)
M = mass of test system $= M_s + M_f$ (kg)
M_s = bearing mass (kg)
M_f = mass of lubricant (feed plenum) (kg)
$M_{s-\alpha\beta}$ = test system inertia coefficients (kg), $\alpha, \beta = x, y$
$M_{\mathrm{SFD}\alpha\beta}$ = squeeze film inertia coefficients (kg), $\alpha, \beta = x, y$
R = radius of squeeze film land (m)
t = time (s)
x and y = bearing motions along X, Y dirs. (m)
$\bar{x}$ and $\bar{y}$ = DFT components of bearing motions (m)
ρ = lubricant density (kg/m^3)
μ = viscosity (Pa s)
ω = excitation frequency (rad/s)

Matrices and Vectors

$\mathbf{C_s}$ = structure (remnant) damping matrix (N s/m)
$\mathbf{C_{SFD}}$ = squeeze film damping coefficients matrix (N s/m)
$\mathbf{F}$ = $[F_x, F_y]^{\mathrm{T}}$ external excitation load vector (N)
$\bar{\mathbf{F}}$ = DFT load vector in frequency domain (N)
$\mathbf{F_{SFD}}$ = **FSFD_V**+**FSFD_I**, squeeze film damper force reaction vector (N)
$\mathbf{F_{SFD\_V}}(t)$ = $-\mathbf{C_{SFD}}\dot{\mathbf{z}}$, $\mathbf{F_{SFD\_I}}(t) = -\mathbf{M_{SFD}}\ddot{\mathbf{z}}$
$\mathbf{K_s}$ = support structure stiffness matrix (N/m)
$\mathbf{M_s}$ = system mass matrix (kg)
$\mathbf{M_{SFD}}$ = squeeze film inertia coefficient matrix (kg)
z = $[x, y]^{\mathrm{T}}$ displacement vector (m)
$\bar{\mathbf{z}}$ = DFT displacement vector in frequency domain (m)

References

[1] Chen, C. S., Natsiavas, S., and Nelson, H. D., 1998, "Coupled Lateral-Torsional Vibration of a Gear-Pair System Supported by a Squeeze Film Damper," Trans. ASME, J. Vib. Acoust., **120**(4), pp. 860–867.
[2] Locke, S., and Faller, W., 2003, "Recycle Gas Compressor Designed for High Unbalance Tolerance and Stability," *Proceedings of the 32nd Turbomachinery Symposium*, Houston, TX, pp. 137–144.
[3] Hibner, D. H., 1975, "Dynamic Response of Viscous-Damped Multi-Shaft Jet Engines," J. Aircr., **12**(4), pp. 305–312.
[4] Hibner, D. H., Kirk, R. G., and Buono, D. F., 1977, "Analytical and Experimental Investigation of the Stability of Intershaft Squeeze Film Dampers," ASME J. Eng. Power, **99**(1), pp. 47–52.
[5] Hibner, D. H., Bansal, P. N., and Buono, D. F., 1978, "Analysis and Experimental Investigation of the Stability of Intershaft Squeeze Film Dampers-2: Control of Instability," ASME J. Mech. Des., **100**(3), pp. 558–562.
[6] El-Shafei, A., 1991, "Stability Analysis of Intershaft Squeeze Film Dampers," J. Sound Vib., **148**(3), pp. 395–408.
[7] Gupta K., and Chatterjee S., 2007, "Dynamics of an Improved Inter Shaft Squeeze Film Damper: Theory and Experiment," ASME Paper No. GT2007-27534.
[8] Chen, S., and Liu, S., 1986, "Equivalent Linearization of a Squeeze Film Damper," ASME J. Vib., Acoust., Stress, Reliab. Des., **108**(4), pp. 434–440.
[9] Defaye, C., Bonneau, O., Arghir, M., and Imbourg, F., 2008, "Dynamic Behavior of a Double Spool Rotor Integrating an Oil-Damped Intershaft Bearing," Tribol. Trans., **51**(5), pp. 562–572.
[10] Tiwari, R., Lees, A. W., and Friswell, M. I., 2004, "Identification of Dynamic Bearing Parameters: A Review," Shock Vib. Dig., **36**(2), pp. 99–124.
[11] Della Pietra, L., and Adiletta, G., 2002, "The Squeeze Film Damper Over Four Decades of Investigations. Part I: Characteristics and Operating Features," Shock Vib. Dig., **34**(1), pp. 3–26.
[12] Della Pietra, L., and Adiletta, G., 2002, "The Squeeze Film Damper Over Four Decades of Investigations. Part II: Rotordynamic Analyses With Rigid and Flexible Rotors," Shock Vib. Dig., **34**(2), pp. 97–126.
[13] San Andrés, L., and Delgado, A., 2007, "Identification of Force Coefficients in a Squeeze Film Damper With a Mechanical End Seal-Centered Circular Orbit Tests," ASME J. Tribol., **129**(3), pp. 660–668.
[14] El-Shafei, A., and Eranki, R. V., 1994, "Dynamic Analysis of Squeeze Film Damper Supported Rotors Using Equivalent Linearization," ASME J. Eng. Gas Turbines Power, **116**(3), pp. 682–691.
[15] Zhang, J. X., and Roberts, J. B., 1996, "A Frequency Domain Parametric Identification Method for Studying the Non-Linear Performance of Squeeze Film Dampers," J. Sound Vib., **189**(2), pp. 173–191.
[16] Ellis, J., Roberts, J. B., and Ramli, M. D., 1989, "The Experimental Determination of Squeeze-Film Dynamic Coefficients Using the State Variable Filter Method of Parametric Identification," ASME J. Tribol., **111**, pp. 255–259.
[17] Roberts, J. B., Ellis, J., and Hosseini, S. A., 1990, "The Determination of Squeeze Film Dynamic Coefficients From Transient Two-Dimensional Experimental Data," ASME J. Tribol., **112**(2), pp. 288–298.
[18] Diaz, S., and San Andrés, L., 1999, "A Method for Identification of Bearing Force Coefficients and Its Application to a Squeeze Film Damper With a Bubbly Lubricant," STLE Tribol. Trans., **42**(4), pp. 739–746.
[19] San Andrés, L., and De Santiago, O., 2004, "Forced Response of a Squeeze Film Damper and Identification of Force Coefficients From Large Orbital Motions," ASME J. Tribol., **126**(2), pp. 292–300.
[20] Zeidan, F. Y., San Andrés, L., and Vance, J. M., 1996, "Design and Application of Squeeze Film Dampers in Rotating Machinery," *Proceedings of the 25th Turbomachinery Symposium*, Houston, TX, pp. 169–188.
[21] Delgado, A., and San Andrés, L., 2008, "Nonlinear Identification of Mechanical Parameters in a Squeeze Film Damper With Integral Mechanical Seal," ASME Paper No. GT2008-50528.
[22] San Andrés, L., 1985, "Effect of Fluid Inertia Effect on Squeeze Film Damper Force Response," Ph.D. thesis, Texas A&M University, College Station, TX.
[23] Vance, J., 1988, *Rotordynamics of Turbomachinery*, Wiley, New York, pp. 240–260.
[24] Delgado, A., 2008, "A Linear Fluid Inertia Model for Improved Prediction of Force Coefficients in Grooved Squeeze Film Dampers and Grooved Oil Seal Rings," Ph.D. thesis, Texas A&M University, College Station, TX.
[25] Rodriguez, L. E., 2004, " Experimental Frequency-Dependent Rotordynamic Coefficients for a Load-On-Pad, High-Speed, Flexible-Pivot Tilting Pad Bearing," MS thesis, Texas A&M University, College Station, TX.